ELSEVIER

Raman phase conjugate resonator
for intracavity aero-optic turbulence aberration correction

V.S. Sudarshanam [a,*], M. Cronin-Golomb [a], P.R. Hemmer [b], M.S. Shahriar [c]

[a] *Electro-Optics Technology Center, 4 Colby Street, Tufts University, Medford, MA 02155, USA*
[b] *Air Force Research Laboratory, Sensors Directorate, Hanscom Air Force Base, Bedford, MA 01731, USA*
[c] *Research Laboratory of Electronics, Massachusetts Institute of Technology, Cambridge, MA 02139, USA*

Abstract

A cw degenerate phase conjugate resonator (PCR) with intracavity aero-optic turbulent flow is demonstrated using sodium vapor pumped with a low intensity cw laser. A turbulent helium jet at a high flow velocity of 250 m/s and forcing frequency of 18 kHz generated the spatio-temporal aberrations. The intracavity normalized peak-to-peak intensity fluctuations at 18 kHz measured with a pinhole-detector are ten times smaller in the corrected beam than in the aberrated beam. The threshold pump intensity for the resonator is ~ 4.5 W/cm^2 in the absence of the turbulent flow. The pump frequency is tuned well within the Doppler width of the Na D$_1$ transition. Evidence of a degenerate (laboratory frame) double-Λ mechanism involving Zeeman sublevels is also shown. © 1999 Published by Elsevier Science B.V. All rights reserved.

1. Introduction

Phase conjugate resonators (PCRs) have many applications ranging from aberration correction and target/source tracking to associative memories, optical data processing, imaging threshold detectors, and one-way image transmission (when used in combination with a phase conjugate mirror, PCM) [1–5]. The practicality of PCMs for these applications depends strongly on the requirements of the nonlinear optic material. Resonant systems, such as sodium vapor are often preferred because they provide gain greater than unity and a response time in the nanosecond regime, even with cw lasers. However, previous cw Na vapor PCRs required high-intensity pump beams, which necessitated strong focusing to spot sizes of ~ 100 μm [6]. This limits applications, especially those related to imaging. In

this paper, we demonstrate a PCR that has 320 times lower resonating threshold (~ 4.5 W/cm^2 pump intensity) than the best previous [6] Na vapor cw PCR. This low threshold intensity allows large diameter cw pump beams to be used and has permitted, for the first time, demonstration of a PCR with fast intracavity aberrations. Phase conjugation through the Zeeman coherence grating mechanism in Na vapor has been used before in a pulsed PCR [7] and cw collinear pump-probe resonator that could not correct for aberrations [8]. More detailed comparison to these reports is summarized in Section 5.

Recently, we showed high-speed, high-gain turbulence aberration correction in a PCM geometry [9] using non-degenerate four-wave-mixing (NDFWM) [10] based on Raman coherent population trapping (CPT) [11,12]. However, to construct a single-frequency PCR, identical frequencies are required for the 'probe' and 'conjugate' beams. This can be achieved by using Raman CPT between the Zeeman sublevels of a single hyperfine transition.

* Corresponding author. E-mail: sudar@mit.edu

2. Mechanism: degenerate PCM

Fig. 1(a) shows a three-level interaction involving the Zeeman sublevels ($m_F = -1$, 0, 1) of the $F = 1$ and $F' = 1$ hyperfine levels of the Na D_1 line. All interacting beams are considered circularly polarized. The forward pump, F, and the probe beam, P, forming a single Λ system are Raman-resonant, thus pumping the atoms into a non-absorbing dark state. This process traps atoms in a coherent superposition of the ground sublevels which is decoupled from the excited state, and is commonly called coherent population trapping (CPT). The prefix Raman is
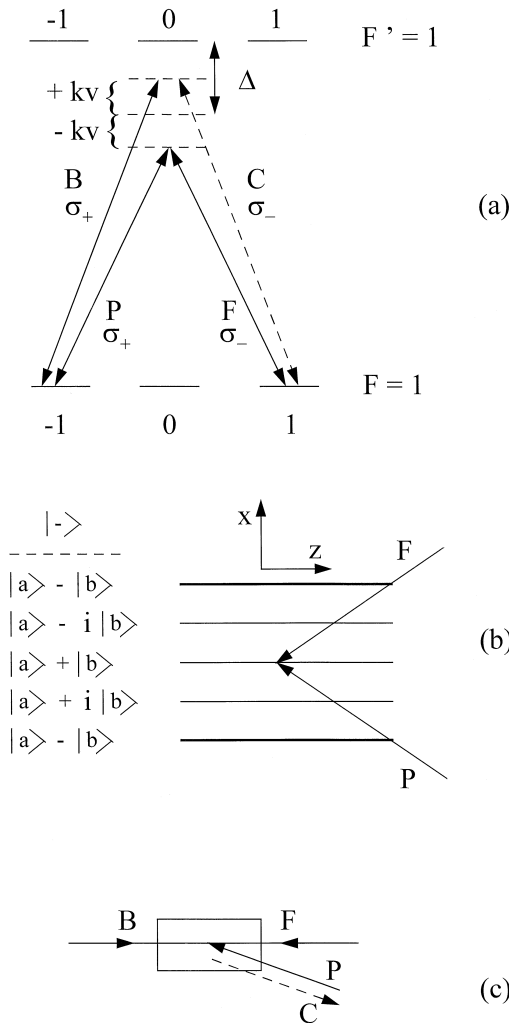

(a)

(b)

(c)

Fig. 1. (a) Schematic level diagram for Raman CPT in a double-Λ system (atom frame) involving the Zeeman sublevels of the $F = 1$ to $F' = 1$ transition of the Na D_1 line. Δ is the laser frequency detuning from the $F' = 1$ level. kv is the Doppler shift for the atom velocity, v. (b) Grating between F and P resulting in spatial dependence of the orientation of ground-state Zeeman coherence. (c) FWM geometry.

added to denote a folded (Λ) three-level system as opposed to the cascade three-level system and the V system [11,12]. For non-collinear propagation of F and P, a grating is formed as shown in Fig. 1(b). The orientation of the Zeeman coherence between the ($m_F = -1$, 1) ground sublevels varies with position along x according to the expression for the dark state,

$$|-\rangle = \frac{1}{\sqrt{2}}\big[|a\rangle\exp(ik_P x) - |b\rangle\exp(ik_F x)\big] \qquad (1)$$

where $|a\rangle$ and $|b\rangle$ denote the two sublevels $m_F = -1$ and 1, respectively. The backward pump, B, diffracts off this Zeeman grating to form the conjugate beam, C, as shown in Fig. 1(c). The Raman-resonant beams B and C form the second Λ system. As explained in Refs. [11,12], the optical pumping mechanism of the Raman CPT saturates the optical nonlinearity (ground state coherence) at an intensity far below that needed to saturate the optical transition. Thus, a high conjugate gain can be obtained in CPT-based FWM using low intensity pumps.

To see how degenerate four wave mixing (DFWM) can be performed using the double-Λ system of Fig. 1(a), transform from the laboratory frame to the atom frame. As shown in the atom frame in Fig. 1(a), the Doppler shift ($\pm kv$) for moving atoms creates a non-degeneracy, even though all laser beams are degenerate in the laboratory frame. Here, we assume that v is along the propagation direction of F, and P is nearly co-propagating to F. For the ($m_F = -1,0,1$) system, linear polarization can be used instead of circular polarization, still maintaining the CPT superposition in the Λ transitions (see Refs. [11,12]).

3. Experimental arrangement and method

In the PCR experimental arrangement shown in Fig. 2, the linearly polarized forward (F) and backward (B) pump beams counterpropagate in the Na vapor cell. The pumps are slightly focused by lenses, L ($f = 1$ m) to a FWHM diameter of 660 μm at the cell center. An optical isolator, I, prevents feedback into the dye laser from reflections. A PCR cavity is formed between the high-reflectivity (95%) output coupler, R, and the Na vapor high-gain PCM. To resonate efficiently, light reflected from the ordinary mirror R must be a plane wave. However, this plane wave will be aberrated (beam A) after passing through the helium jet and so must be phase conjugated in the Na cell to produce a corrected beam C after passing back through the helium jet. The portion of A transmitted through the cell is denoted by 'T'. In the degenerate Na PCM, the conjugate beam is generated primarily by the scattering of B from the grating formed by F and A. The DFWM interaction excites Raman transitions among Na magnetic sublevels. This gives a PCR beam that is nominally cross-polarized relative to both F and B. Because of this cross-polariza-
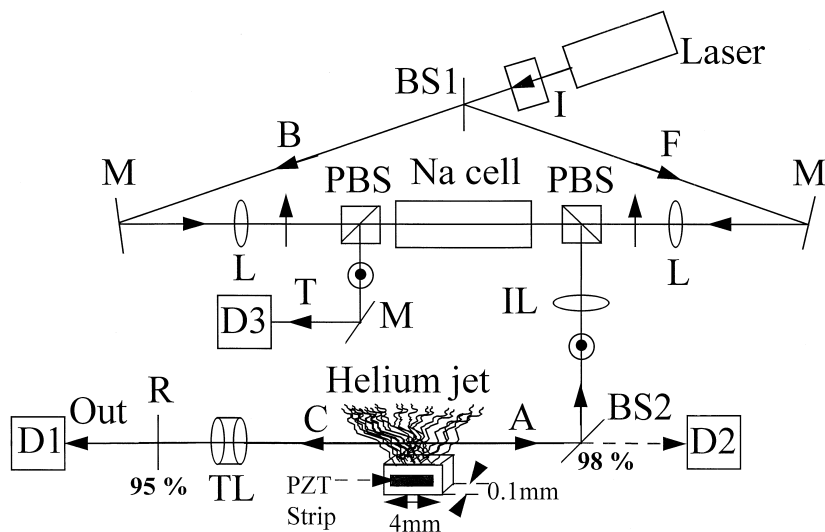
Fig. 2. Schematic of the experimental arrangement for a degenerate PCR with intracavity turbulence aberration correction.

tion, polarizing beam splitters, PBS, can be used to facilitate the steering of A into the cell, and to better separate C from B. The PBSs are not required to operate the PCR or maintain cross-polarization between the pumps and PCR beams. The PCR beams A and C are aligned to intercept F and B in the cell at a vertical angle of ~ 8.5 mrad. In the absence of turbulence, beam A (and C) has a diameter of ~ 0.23 mm at the center of the cell. A telescope, TL, compensates diffraction effects in the PCR cavity. The typical optical intensity of F and B at the cell center is about 10 W/cm^2 each, unless otherwise stated. The intensity of C (or A) at the cell center is estimated to be ~ 2.6 W/cm^2 at the maximum intracavity PCR power of 1.7 mW. The Na vapor cell is a heat-pipe oven operated at $\sim 260°$C with an ambient pressure of ~ 18 mTorr. No buffer gas is added to the cell. Stray magnetic fields are reduced to less than 20 mG with the use of magnetic shielding around the cell.

The turbulent jet is placed 1 m away from the imaging lens, IL ($f = 25$ cm) which images it into the cell with a demagnification of $\sim 67\%$. This jet is obtained by forcing helium gas at room temperature through a rectangular nozzle (4 mm $\times$ 0.1 mm) placed ~ 3 mm below the PCR beam path. The nozzle is acoustically driven by a PZT transducer at the flow resonance frequency of 17.8 kHz. The average helium flow speed at the nozzle exit is estimated to be ~ 250 m/s.

To demonstrate spatial aberration correction, the profile of C is sampled by the CCD camera (D1) and the profile of A is sampled by D2. The D1 camera is placed 1.92 m away from the jet, and D2 is 0.57 m away from the jet. Temporal aberration is measured by replacing D1 (and D2) by a 0.3 mm pinhole mounted on a photodetector (PPD). The transverse location of the PPD is adjusted for maxi-

mum amplitude of the 17.8 kHz intensity variation caused by the turbulence. The ratio of the peak-to-peak intensity variation to the maximum intensity level is defined as the modulation depth. This allows an intensity-independent comparison of the temporal aberrations in beams C and A.

4. Results and discussion

Spatial aberration correction is demonstrated in Fig. 3 through (time-averaged) CCD images. The beam profiles are shown both as two-dimensional contour plots at intervals of 20% of the peak intensity, and as one-dimensional line traces made near the vertical center of each profile. The profile of A, sampled by D2, is shown in Fig. 3(a) with the helium flow ON and OFF (left and right profiles respectively), while that of C, sampled by D1 is shown in Fig. 3(b) under corresponding flow conditions. As seen from Fig. 3(a) and Fig. 3(b), a well-corrected nearly-circular spot is seen at the output coupler R on double-pass through the jet, whereas A is severely aberrated by the helium jet. The difference in the sizes of the beams C and A shown in Fig. 3 is due to the magnification by the telescope, TL. The profile of the transmitted PCR beam, T, is sampled by camera D3 which is 0.54 cm away from the cell center (see Fig. 2) and is shown in Fig. 3(c) with the flow ON and OFF. As expected, T is aberrated by the flow in like manner to A.

Fast temporal aberration correction at 17.8 kHz is demonstrated in Fig. 4 through plots of the instantaneous output voltage from the PPD. Here, Fig. 4(a) shows the effect of turbulence on the aberrated PCR beam A, while Fig. 4(b) shows that for the compensated PCR beam, C. From this data, the signal modulation depth in A is esti-
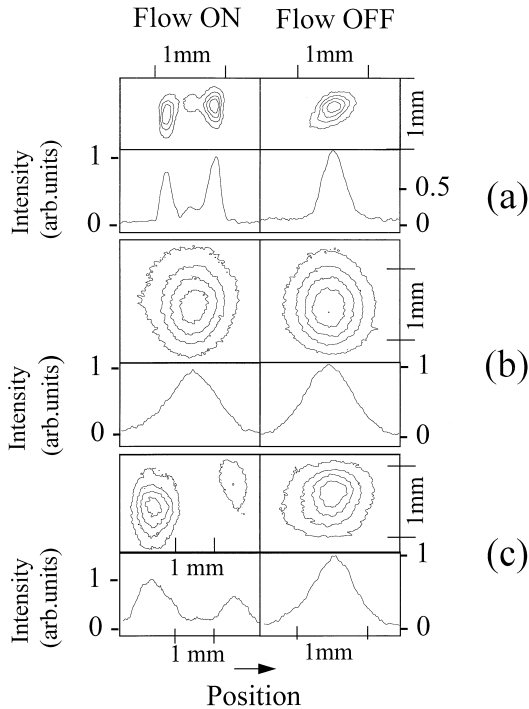
Fig. 3. Data showing spatial aberration correction: 2-D contours (upper plots) and 1-D line traces (lower plots) of the intensity profile of (a) the aberrated PCR beam, A, (b) the compensated PCR beam, C and (c) the transmitted PCR beam, T. Contour lines are drawn at 80, 60, 40 and 20% of peak intensity.

mated at $\sim 63.6\%$ whereas that in C is $\sim 6.6\%$, demonstrating that temporal fluctuations are reduced by a factor of ~ 9.6 in the PCR beam near R.

In order to establish that the system is indeed based on purely DFWM and not NDFWM as in Ref. [10], the optical frequency of C (and A) is determined by beating with a probe beam, P (not shown in Fig. 2) that is shifted
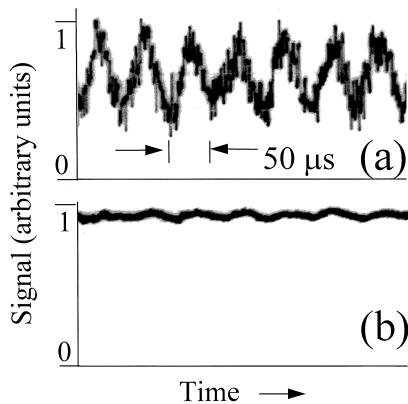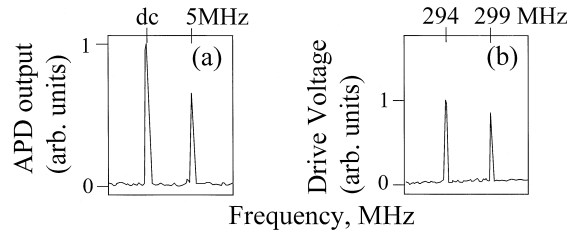

Fig. 5. Verification of DFWM: (a) the optical beat between C (or A) and the probe P (shifted by 5 MHz from F), and (b) the electrical voltage spectrum of the two AOM drive signals at 294 and 299 MHz used to generate P.

by 5 MHz relative to F. Fig. 5(a) shows the output frequency spectrum of an avalanche photodiode (APD) on which the two beams C (or A) and P are beat. Fig. 5(b) shows the electrical spectrum of the two AOM drive signals. The agreement between the optical and electrical frequency shifts in Fig. 5(a,b) establishes that DFWM indeed gives rise to C and A. The single PCR peak seen from Fig. 5(a) shows that the PCR is oscillating in a single longitudinal mode even without any intracavity frequency-selective elements. For the cavity length of 2.1 m, the expected [2] PCR longitudinal mode spacing ($c/4L$) is ~ 36 MHz. Multiple longitudinal modes are not supported in our PCR because the two-photon bandwidth of the CPT interaction is far less, as discussed later.

Fig. 6(a) shows the intracavity optical power as a function of the pump frequency. The peaks named I, J and K can be selectively enhanced in power at their respective frequencies by changing the alignment angle between C (A) and the pumps F and B. Aberration correction measurements described in this paper are done with the peak I enhanced as it occurs at the largest angle of ~ 8.5 mrad from the pumps. This also avoids the conical emission [6,13] that occurs near the peak K. The conical emission near peak K has a typical half-angle of ~ 5 mrad and has

Fig. 4. Temporal aberration correction: PPD signal showing turbulence effects on (a) aberrated PCR beam, A and (b) the compensated PCR beam, C.
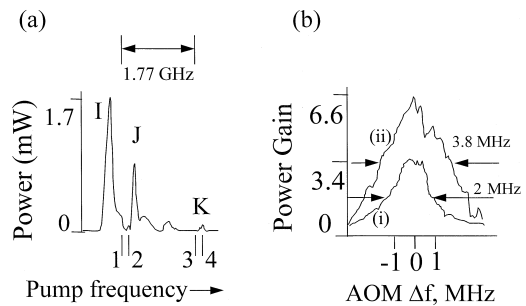

Fig. 6. (a) PCR intracavity power as a function of the pump frequency. The numbers 1 through 4 correspond to the following D_1 transitions: (1) $F = 2 \leftrightarrow F' = 1$, (2) $F = 2 \leftrightarrow F' = 2$, (3) $F = 1 \leftrightarrow F' = 1$, and (4) $F = 1 \leftrightarrow F' = 2$. (b) The PCM conjugate gain as a function of Δf for the two pump intensities (i) 4.6 W/cm^2 and (ii) 10 W/cm^2.

a characteristic hexagonal pattern. The small broadened peaks between J and K are from diffuse conical emission that is primarily orthogonal in polarization to C (and A). The peak I is enhanced when the pump laser frequency is red-detuned by ~ 300 MHz from the $F = 2$ to the $F' = 1$ transition. It should be noted that the Doppler width of Na vapor at 260°C is ~ 1.1 GHz. Therefore, the detuning measured applies only to the zero-velocity group in the vapor.

The threshold pump intensity at which the PCR output becomes unstable in time was determined (with the flow OFF) by attenuating the total pump power obtained from the laser. The laser frequency was kept fixed at the peak I shown in Fig. 6(a). The threshold intensity for each pump was found to be 4.5 W/cm². The helium flow reduced the intracavity PCR power to half its value without flow. Thus, the threshold pump intensity would be correspondingly higher with the flow ON.

To test for CPT, a probe beam, P, with variable frequency relative to F is conjugated, with the output coupler R misaligned to stop oscillation of the PCR. However, other experimental operating conditions remain unchanged. The pump laser is tuned to the peak I and the difference frequency, Δf, between P and F is varied using the set of two AOMs described earlier. Fig. 6(b) shows the conjugate power gain (probe power ~ 90 μW) as a function of the difference frequency between F and P, for two different pump intensities. The FWHM of the gain is ~ 2 MHz for the lower pump intensity, which is far less than the 10 MHz excited state decay rate of Na. This subnatural difference-frequency linewidth for the two-photon interaction is taken as direct evidence for Raman CPT. Another test [9–12] for Raman CPT is the dependence of the FWHM on the generalized two-photon Rabi frequency (which is proportional to pump intensity). The linewidth increases from 2 MHz to 3.8 MHz when the pump intensity increases from 4.6 W/cm² to 10 W/cm². In order to test the double-Λ nature of the CPT-based DFWM interaction [9] the conjugate and the probe beams are beat on an APD. When P is shifted by 1 MHz from F (and B), the conjugate beam is found shifted by 2 MHz from P, and by 1 MHz from F (and B).

The phase conjugate response time can be estimated from the reciprocal of the two-photon linewidth and is found from Fig. 6(b) to be ~ 50 ns. This is much faster than the time period (~ 56 μs) of the jet modulation. Spatial aperturing is a likely cause for limited aberration correction ability.

5. Comparison with other reports

Since Na vapor has been used in other PCRs reported in the past [6–8], we make a detailed comparison in Table 1. The experimental conditions of our PCR are designed to optimize the Zeeman coherence amplitude. For example,

Table 1
Comparison of our Zeeman-PCR with other resonators

	Ref. [6]	Ref. [7]	Ref. [8]	This work
Laser type	cw	*Pulsed*	cw	cw
Laser power	*High*	*High*	*High*	Very low
Na transition	D_2	D_1	D_1	D_1
Pump detuning	*1–3 GHz*	*5 GHz*	*4.5 GHz*	300 MHz
Zeeman reflectivity	*Low*	High	High	High
F–B polarizations	Parallel	*Crossed*	Parallel	Parallel
F–P polarizations	*Parallel*	Crossed	Crossed	Crossed
P–C polarizations	Parallel	*Crossed*	Parallel	Parallel
F–P angle	Non-zero	Non-zero	*Zero*	Non-zero

Words in *italics* denote a difference compared to our work.

F denotes the forward pump forming grating with the probe (or resonator/PCR) beam, P.

B denotes the backward pump which diffracts off the F–P grating to form the conjugate beam, C.

tune the pumps well within the Doppler width, use the D_1 transition instead of the D_2 transition, use co-polarized pumps which generate cross-polarized PCR beams, and a phase conjugate geometry with non-zero angle between the pump and PCR beams. The Na cell is also optimized for temperature, background pressure and interaction length. For example, a 10°C change in cell temperature from 260°C reduced the PCR output by 40% in our case. It can be seen from Table 1 that each of the other reports differ from our work in at least three characteristics, with the most significant and common difference being large detuning. As explained in Ref. [6], the motivation for using a large detuning ($\Delta > 1$ GHz) is based on a homogenously broadened two-level atom model in which the PC reflectivity increases indefinitely, as Δ^2, if the pump intensity and the atomic density can each be increased as Δ^2. However, as explained in Section 2, Raman CPT involves three-level atoms and overcomes the large absorption at smaller Δ, so that correspondingly reduced pump intensity can be used. For example, in Ref. [7], high pump intensity and large detuning were used, and the cross-polarized F and B beams mandated an intracavity quarter-wave plate for PCR action. In Ref. [8], there was a distributed feedback contribution in a collinear pump-resonator geometry that prevented pure PCR action, making it unsuitable for intracavity aberration correction.

6. Conclusion

A low-threshold PCR based on DFWM involving double-Λ CPT interaction has been presented. The intracavity turbulence from a helium jet was modulated at 18 kHz with a flow speed of 250 m/s. The peak-to-peak temporal fluctuations at 18 kHz relative to the maximum signal level have been reduced at the PCR output to one-tenth the intracavity fluctuation. High-fidelity spatial aberration cor-

rection was also demonstrated. Recently [14], potential applications such as frequency standards, intracavity spectroscopy, and optical magnetometery have been proposed for intracavity CPT.

Acknowledgements

References

[1] R.A. Fisher (Ed.), Optical Phase Conjugation, Academic, New York, 1983, Chaps. 13 and 14.

[2] R.C. Lind, D.G. Steel, Opt. Lett. 6 (1981) 554.

[3] A. Yariv, S.-K.K. Kwong, Opt. Lett. 11 (1986) 186.

[4] G.J. Dunning, S.W. McCahon, M.B. Klein, D.M. Pepper, J. Opt. Soc. Am. B 11 (1994) 339.

[5] M.B. Klein, G.J. Dunning, G.C. Valley, R.C. Lind, T.R. O'Meara, Opt. Lett. 11 (1986) 575.

[6] J.R.R. Leite, P. Simoneau, D. Bloch, S. Le Boiteux, M. Ducloy, Europhys. Lett. 2 (1986) 747, for the estimated beam waist, see Ref. [10] below.

[7] E. Le Bihan, M. Pinard, G. Grynberg, Opt. Lett. 11 (1986) 159.

[8] M. Vallet, M. Pinard, G. Grynberg, Opt. Commun. 81 (1991) 403.

[9] V.S. Sudarshanam, M. Cronin-Golomb, P.R. Hemmer, M.S. Shahriar, Opt. Lett. 22 (1997) 1141.

[10] P.R. Hemmer, D.P. Katz, J. Donoghue, M. Cronin-Golomb, M.S. Shahriar, P. Kumar, Opt. Lett. 20 (1995) 982.

[11] E. Arimondo, in: E. Wolf (Ed.), Progress in Optics XXXV, Elsevier, New York, 1996, pp. 258–354.

[12] H.R. Gray, R.M. Whitley, C.R. Stroud, Opt. Lett. 3 (1978) 218.

[13] G. Grynberg, E. Le Bihan, P. Verkerk, P. Simoneau, J.R.R. Leite, D. Bloch, S. Le Boiteux, M. Ducloy, Opt. Commun. 67 (1988) 363.

[14] M.D. Lukin, M. Fleischhauer, M.O. Scully, V.L. Velichansky, Opt. Lett. 23 (1998) 295.